ISSN NO. 2320-5407

Journal homepage: http://www.journalijar.com

INTERNATIONAL JOURNAL OF ADVANCED RESEARCH

RESEARCH ARTICLE

Spine Image Fusion Via Weighted Algorithm of Pixel Level

V. Sathiya Jeyaseel, S. Sivasangumani, M. Savitha
M.E Applied Electronics, ECE Department, V. S. B Engg College, Karur , TamilNadu.
sathiyavincent@gmail.com, sivasangumani@gmail.com, savithabme@gmail.com

Manuscript Info

Manuscript History:

Received: 15 November 2013
Final Accepted: 22 December 2013
Published Online: January 2014

Key words:
Medicalimaging,spine,weighting algorithm , graph cuts, RMSE.

Abstract

The different imaging modality of spine image fusion has been increased in the medical field for the purpose of getting more information regarding spine reordering and bone fracture. CT and MRI of the spinal cord provide complementary information of possible relevance for diagnostic and therapeutic decisions. This article investigates a novel CT/MR spine image fusion based on weighting algorithm of pixel level. This algorithm allows physicians to visually assess corresponding soft tissue and bony detail on a single image eliminating mental alignment and correlation needed when both CT and MR images are required for diagnosis. The proposed weighting algorithm for fusion guarantees nearly global solutions, while avoiding the pix elation artifacts that affect standard wavelet-based methods. We further introduce a transparency-labeling formulation, which significantly reduces the computational load in spine image fusion. Graph cuts algorithm has been introduced to allocate the weighting factor for the particular pixel. Combining Graph cuts and weighting algorithm leads to energy minimization in fusion environment. The image fusion quality has been evaluated by consistency verification , mutual verification , RMSE.

Introduction

Radiologists currently display MR and CT images side by side, when both images are available. This does provide them with all the available image information, but its accessibility is limited to visual correlation between the
two images. It can be difficult to determine whether narrowing of a spinal canal is caused by a tissue or bone from clinical MR images: hence, both CT and MR can be
employed . Using both CT and MR images, as opposed to relying on a single modality can benefit diagnosis and treatment of osteophytes and degenerate discs that impact bone and nerve structures. In addition, both modalities can aid postoperative follow up after the spinal surgery. Here, both the CT and MR modalities provide complementary information.

Here, we present a novel method for image fusion of the spine, which preserves the bone structures and soft tissue detail in a single image. Multimodality image fusion has been studied in other fields, with applications varying from multifocal to geographical images . In medicine, image fusion has been used for brain imaging , MRI-SPECT fusion , epilepsy treatment planning , liver ablation , and digital subtraction angiography . For the spine, registered and overlaid CT and MR spine images have been used for surgery planning , and evaluation of bone implants . A wavelet-based approach to image fusion has been proposed by Li *et al.*. The two input images were fused in the wavelet domain, and an inverse trans-formation was applied to produce the result. Other variations of this technique include additive wavelet decomposition , the contourlet transform , the curvelet transform [16], and the complex wavelet transform . The wavelet or transform-based methods can suffer from pixelation artifacts when two dissimilar images are fused. This is a result of the decimations involved in the wavelet transform as well as the translation dependence of standard wavelets. This may result in small details being distorted, leading to a significant loss in image quality. Pathologies that should have been

visible may no longer be seen.

In this study, we state image fusion as a discrete multilabel optimization problem, which can be solved efficiently with graph cuts , via the well-known swap or alpha-expansion moves . The proposed energy function balances the contributions of three competing terms: 1) a squared error, which encourages the solution to be similar to the MR input, with preference to strong MR edges; 2) a squared error, which encourages the solution to be similar to the CT input, with preference to strong CT edges; and 3) a prior, favoring smooth solutions by encouraging neighboring pixels to have similar fused-image values. We further introduce a transparency-labeling formulation, which significantly reduces the computational load. The proposed graph-cut fusion guar-antees nearly global solutions, while avoiding the pixelation artifacts that affect standard wavelet-based methods. We report several quantitative evaluations/comparisons over 40 pairs of CT/MR images acquired from 20 patients. The results demon-strate very competitive performance in comparisons to existing variational and transform based methods.

2. IMAGE FUSION TECHNIQUE

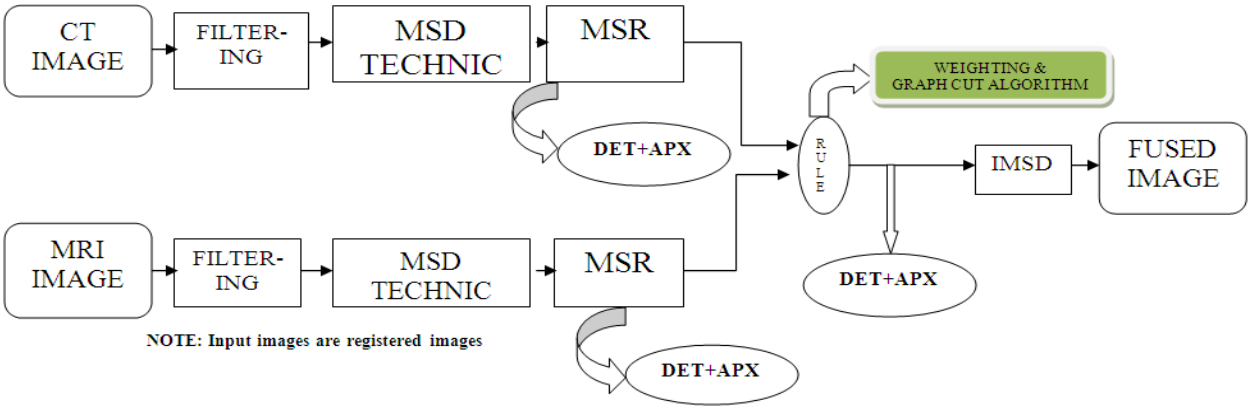

Fig 1. Fusion technique

The fig.1 shows the entire operation of image fusion, Both the input images are applied into the per-processing technique such as image registration and filtering. And then decompose into high frequency and low frequency component(DET and APX respectivily). And apply the weighting factor based on the pixel coefficient value of the multiscale representation. Based on the weighting factor and pixel value the pixels are segregated into different label. Each label having unique characteristics, the different labels are addressed into graph cuts algorithm. The graph cuts algorithm which is reduces the distance between image pixels, So that we can achive the energy minimization in the fusion environment.

3.STEPS INVOLVED IN IMAGE FUSION

STEP1: *Applying filtering process and registration to the MRI and CT image.*
STEP2: *Decompose the input images into low and high pass coefficient such as Approxima-tion and detailed (V,H,D) MSR'S using SWT.*
STEP3: *Split the coefficients in the MSR'S according to the pixel value and similarity of the pixels and create the labels.(each label contain similar pixel characters)*
STEP4: *Each labels introduced into graph cuts algorithm.*
STEP5: *Applying the weighting factor to the different labels output.*
STEP6: *Fuse the each image labels with weighting factor.*
STEP7: *Evaluate the fusion quality using RMSE,PSNR,SSIM*

4.PROBLEM FORMULATION

A. Registration and Preprocessing

The input volumes were registered, using a rigid 3-D versor-based transform in ITK [33]. The optimizer used maximiza-tion of mutual information (MI) [34] to align soft tissue details present in both images (note the soft tissue details in the CT image are suitable for registration, but MR is better for diagno-sis). For the purpose of aligning soft tissue each CT image was thresholded from −255 to 255 Houndsfield Units (HU) or −255 to 0 HU if needed. This kept

many of the soft tissue details, but removed most of the bone detail. Both images were then scaled to an intensity range of 0 to 255 to be in the same range. The transform was initialized using two corresponding user-selected points, one from the CT and the other from the MR image. After this, MI was calculated from the voxels in both images, and the versor transform was iteratively updated based on MI of the two images at each step. Using the obtained optimal transform, the original MR image (without intensity scaling) was transformed and resampled to the voxel spacing of the CT image.

Manual points were selected in the 3-D images for the target registration error (TRE) and the fiducial localization error (FLE) evaluation. The TRE is the mean post-registration Euclidean distance between corresponding pairs of fiducials from the input images. The FLE is the root mean squared difference in locations when selecting the same fiducial multiple times in an image [35]. The TRE used 17 points from two image pairs. For the FLE, five distinct points were defined on the CT image. On five separate days, corresponding points in the MR image were identified producing a total of 25 point sets. These errors were used to validate the registration.

After registration, the original CT images were thresholded at 0 HU, setting any negative values to 0 HU and leaving other values unchanged. This removed most of the soft-tissue details and was done because the MR presents the tissue detail with more clarity, so the CT tissue detail is undesirable for the fused image. For all 20 patients, the MR images were found to have a maximum intensity of about 700, and the CT images were found to have a maximum intensity of about 1400. In view of this, the CT intensities were divided by two so that the MR and CT histograms would have similar intensity ranges prior to fusion. This was needed to eliminate bias in the fusion algorithm due to differing intensity ranges in the input images. MR and CT histograms are shown in Fig. 2, while Fig. 3 shows a flow chart describing the registration and preprocessing steps.

B. Median Filter

The median filter is a nonlinear digital filtering technique, often used to remove noise. Such noise reduction is a typical pre-processing step to improve the results of later processing (for example,edge detection on an image). Median filtering is very widely used in digital image processing because, under certain conditions, it preserves edges while removing noise .

C. *SWT decomposition*

Stationary wavelet transform is first performed on each source images, and then a fusion decision map is generated based on a set of fusion rules. The fused wavelet coefficient map can be constructed from the wavelet coefficients of the source images according to the fusion decision map. Finally the fused image is obtained by performing the inverse stationary wavelet transform [5]. Let A (x, y) and B (x, y) are images to be fused, the decomposed low frequency sub images of A (x, y) and B (x, y) be respectively lAJ (x, y) and lBJ (x, y) (J is the parameter of resolution) and the decomposed high frequency sub images of A (x,y) and B(x,y) are hAjk (x, y) and hBjk (x, y). (j is the parameter of resolution and j=1,2,3….J for every j, k=1,2,3..). Then, the fused high and low frequency sub-images Fjk (x, y) are given as Fjk (x, y) = Ajk (x, y) if G(Ajk (x, y)) >= G(Bjk (x, y)), else Fjk (x, y) = Bjk (x, y) and FJ (x, y) = lAJ (x, y) if G(AJ (x, y)) >= G(BJ (x, y)), else FJ (x, y) = lBJ (x, y) where G is the activity measure and Fjk (x,y) & FJ (x, y) are used to reconstruct the fused image F′(x, y) using the inverse stationary wavelet transform.

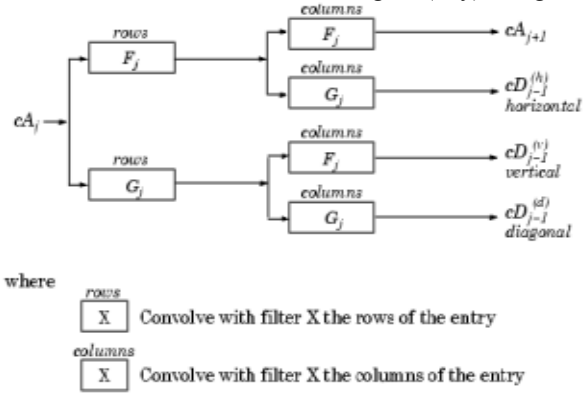

Fig 2: SWT decomposition

D.Weighting algorithm

1.Pixel level Average method

This technique is a basic and straight forward technique and fusion could be achieved by simple averaging corresponding pixels in each input image as:

$$I(a,b) = \frac{I1(a,b) + I2(a,b)}{2}$$

2.*Pixel level Weighted average method*

We add some weights to the individual images and perform the averaging technique as follows:

$$I(a,b) = \frac{W1 * I1(a,b) + W2 * I2(a,b)}{W1 + W2}$$

where W1 and W2 are the weights.

E.Graph cuts

An illustration of the multilabel graph-cutproblem is provided in Fig. 3 . Exactly one label is given to each pixel in the image, with associated data and smoothness costs assigned to the links in the graph. To formulate this optimization let *G = (V, E)*be a weighted graph, with *V* a set of nodes and*E* a set of weighted edges. *V* contains a node for each pixel inΩ and for each label in *Lα* . There is an edge *e{p,q}* between every pair of nodes *p, q*. A cut $C \subset E$ is a set of edges that separates all the label nodes from each other, thereby, creating asubgraph for each label. The minimum-cut problem consists offinding a cut *C* with the lowest cost. The cost of this minimumcut, denoted |*C*|, equals the sum of the edge weights in *C*. By properly setting the weights of the graph, one can use a series of swap moves from combinatorial optimization to efficiently compute the minimum-cost cuts corresponding to a minimum of functional *E*

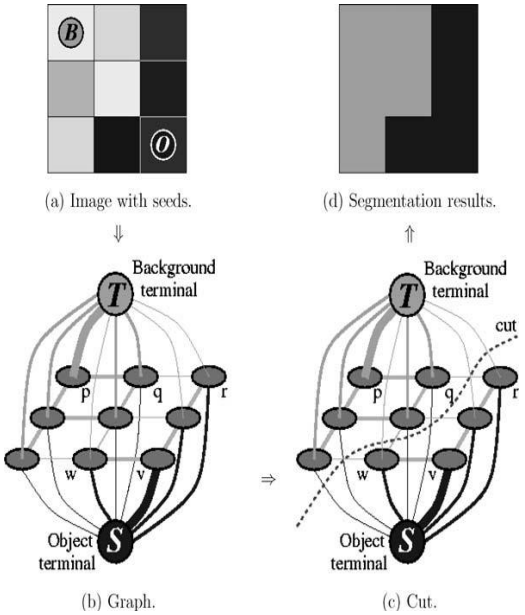

Fig. 3 multilabel graph-cut problem

A swap move starts with a labeled graph and determines for a given pair of labels, *p* and *q*, whether each node having a value in *p, q* should 1) retain its current label or 2) be updated to the other label in the pair. Each swap is accomplished globally in an exact manner by finding the minimum cut on a binary graph consisting of only two labels. This can be extended to the multilabel case by iterating over the set of all possible pairs of labels. The minimum cut is selected at each stage, with the final labeling corresponding to a minimum of the energy functional. One can also use alpha-expansion moves to optimize energy functions of the form *E*. It is well- known that alpha-expansion moves

guarantee a solution that is within a constant factor of the global optimum [26]. However, experimentally, it is well established that swap moves outperform alpha expansions.

5. EVALUATION CRITERIA

Objective image quality measures play an important role in various image processing applications. There are different types of object quality or distortion assessment approaches. The fused images are evaluated, taking the following parameters into consideration.

A. Mean Square error (RMSE)

The root mean square error (RMSE) between each unsharpened MS band and corresponding sharpened band can also be computed as a measure of spectral fidelity. It measures the amount of change per pixel due to the processing.

The RMSE between a reference image R and the fused image F is given by

$$E1 = \sqrt{\frac{1}{MN}\sum_{i=1}^{M}\sum_{j=1}^{N}\left(R(i,j) - F(i,j)\right)^2}$$

There are different approaches to construct reference image using input images. In our experiments, we used the following procedure to compute RMSE.

First, RMSE value El is computed between source image A and fused image F.

$$E1 = \sqrt{\frac{1}{MN}\sum_{i=1}^{M}\sum_{j=1}^{N}\left(I1(i,j) - F(i,j)\right)^2}$$

Similarly E2 is computed as RMSE between source image B and fused image F.

$$E2 = \sqrt{\frac{1}{MN}\sum_{i=1}^{M}\sum_{j=1}^{N}\left(I2(i,j) - F(i,j)\right)^2}$$

Then the overall RMSE value is obtained by taking the average of E1 and E2.

$$RMSE = \frac{(E1+E2)}{2}$$

Smaller RMSE value indicates good fusion quality. Peak Signal to Noise Ratio
PSNR can be calculated by using the formula

$$\text{PSNR} = 20\log_{10}\left[\frac{L^2}{MSE}\right]$$

Where MSE is the mean square error and L is the number of gray levels in the image.

B. Image Quality Index

IQI measures the similarity between two images (I1 & I2) and its value ranges from -1 to 1. IQI is equal to 1 if both images are identical. IQI measure is given by

$$IQI = \frac{m_{ab}}{m_a m_b}\frac{2xy}{x^2+y^2}\frac{2m_a m_b}{m_a^2+m_b^2}$$

Where x and y denote the mean values of images I1 and I2 and m^2 , m_b^2, and m_{ab} denotes the variance of I1 , I2 and covariance of I1 and I2.

C.Mutual Information

Mutual Information (MI) measures the degree of dependence of two images. Its value is zero when I1 and I2 are independent of each other. MI between two source images I1 and I2 and fused image F is given by

$$MI = \sum_{(f,a)} P_{FA}(f,a) \log_2 \frac{}{P_F(f)P_A(a)} + \sum_{(f,b)} P_{FB}(f,b) \log_2 \frac{P_{FA}(f,b)}{P_F(f)P_b(b)}$$

and $P_A(a)$,$P_B(b)$ and $P_F(f)$ are histograms of images A, B and F,$P_{FA}(f,a)$ *and* $P_{FB}(f,b)$ are the joint histograms of F and A, and F and B respectively. Higher MI value indicates good fusion results.

6. STATISTICAL EVALUATION OF THE FUSED IMAGES

We compared each of the MR and CT images to the fused result within: 1) the regions of soft tissues, and 2) the regions of bone structures. The soft-tissue details consisted of the discs, nerves, and cerebral spinal fluid from the MR image, and the bone details were from the CT image, with a specific focus on the bone cortex. The trabecular bone does not contact soft tissue, and so was omitted. We created image masks of the tissue and bone details for each patient. The tissue masks were created by manual segmentations of the MR images, and the bone masks were obtained by thresholding the CT images at a user selected HU for each image and then manually correcting any errors. Fig. 4 shows sample masks of the tissue and bone detail. We defined a fusion error as the mean absolute-value difference between the MR/CT images and the fused images in the tissue regions defined by the masks. For the MR images, we calculated the following two errors

$$e_{\mathrm{MR,Tissue}} = \frac{\sum_{M_{\mathrm{Tissue}}} |I_{\mathrm{MR}} - I_{\mathrm{fused}}|}{\text{area of the tissue mask}}$$

$$e_{\mathrm{MR,Bone}} = \frac{\sum_{M_{\mathrm{Bone}}} |I_{\mathrm{MR}} - I_{\mathrm{fused}}|}{\text{area of the bone mask}}$$

where *I*MR is the intensity of the MR image for a given pixel, *I*fused is the intensity of the fused image at a given pixel and *M*Tissue ,*M*Bone are the nonzero domains of the two masks. Similarly, two additional errors, *e*CT,Bone and *e*CT,Tissue were defined for the CT images. Ideally, there should be no tissue differences between theMR images and the fused images in the tissue regions (*e*MR,Tissue = 0) and no bone difference between theCT images and the fused images in the bone regions (*e*CT,Bone = 0). The hypothesis we tested was that the error obtained for the MR images is lower than the one obtained for the CT images within soft-tissue regions, i.e., *e*MR,Tissue < *e*CT,Tissue , and higher within bone regions *e*MR,Bone > *e*CT,Bone . Each of the four errors were calculated for each patient. Some of the data were found to be nonnormal using a Shapiro–Wilks test ; thus, a non-parametric Wilcoxon test was used to compare sets of errors. The tissue errors: *e*MR,Tissue and *e*CT,Tissue were compared to each other and the bone errors: *e*CT,Bone and *e*MR,Bone , were also compared, in order to determine if there was a statistical significance difference between them for the 40 patient image sets. These calculations were performed for each of the five fusion methods using version 20 of the SPSS statistical software (SPSS Inc., an IBM Company, Armonk, NY, USA).

7. ADDITIONAL METRICS FUSION FOR EVALUATION

In addition to the above statistical tests, we have also examined the sensitivity and specificity or our algorithm along with the structural similarity in the masks [38]. For classification, we have defined true and false positives/negatives (TP, FP, TN, FN) per pixel as:

1) TPtissue and TNbone if (*e*MR,Tissue < *e*CT,Tissue);
2) FPtissue and FNbone if (*e*MR,Tissue ≥ *e*CT, Tissue);

3) TNtissue and TPbone if (*e*MR,Bone > *e*CT,Bone);
4) FNtissue and FPbone if (*e*MR,Bone ≤ *e*CT,Bone).

Sensitivity and specificity were calculated for each using the total number of TPs, FPs, TNs, and FNs normalized over the image masks, which we denote by *n*TP, *n*FP, *n*TN, and *n*FN. Sensitivity and specificity are defined in (12). Since the tissue sensitivity is equal to the bone specificity and the bone sensitivity is equal to the tissue specificity, only the two sensitivity values have been reported

$$\text{Sensitivity} = \frac{\overline{n}\text{TP}}{\overline{n}\text{TP} + \overline{n}\text{FN}}$$

$$\text{Specificity} = \frac{\overline{n}\text{TN}}{\overline{n}\text{TN} + \overline{\text{n}}\text{FP}}.$$

The structural similarity metric is defined as

$$\text{SSIM}(x, y) = \frac{(2\mu_x\mu_y + C_1)(2\sigma_{xy} + C_2)}{(\mu_x^2 + \mu_y^2 + C_1)(\sigma_x^2 + \sigma_y^2 + C_2)}$$

where μx, μy, σx, σy, σxy represent the means in the x and y images, the variances in the x and y images and the covariance of the two images, respectively. This metric has been applied over a local window for pixels within the given masks, comparing the MR images to the fused images in the tissue mask, and the CT images to the fused images in the bone masks. The window was defined as an 11×11 Gaussian kernel with $\sigma = 1.5$. $C1 = 0.01$ and $C2 = 0.03$ are positive constants.

8. RESULTS

We have taken a spine image to evaluate the results by weighting method with graph cuts.

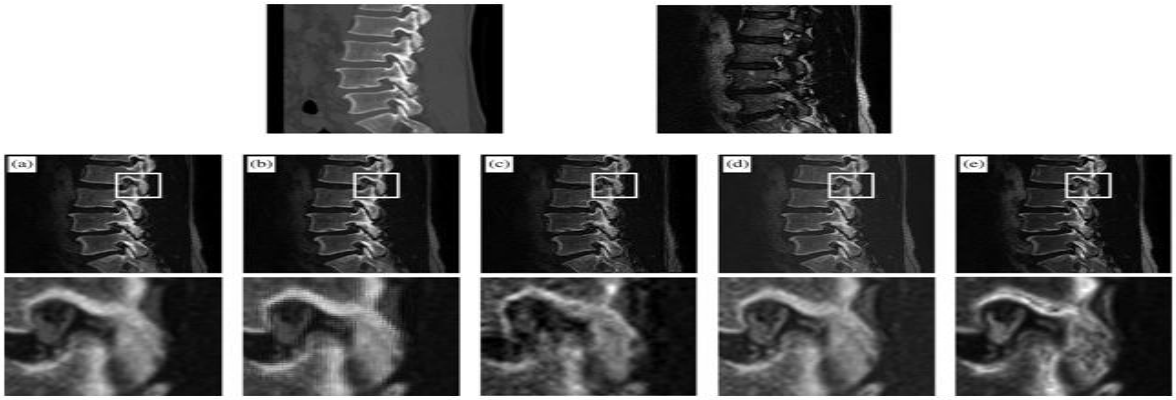

Fig. 4 Sample fused Images: (top left) input CT, (top right) input MR. Middle fused images: (a) averaging method, (b) discrete wavelet transform, (c) contourlet, (d) Piella's variational method, and (e) our proposed weighting and graph-cut method. Bottom row: Magnified images within the region of interest indicated in the images above.

Fig.5 Images of bony spur formation: left - the CT image shows the osteophyte, but not the soft tissue ; middle - in the MR, the osteophyte is not identifiable; right - in the fused image, the osteophyte is clearly visible along with the surrounding soft tissue.

Table1: MEAN FUSION ERROR VALUES FOR THE 20 PATIENT DATA SETS AND STATISTICAL-SIGNIFICANCE TEST RESULTS FOR THE FUSION METHODS

Method	$e_{MR,Tissue}$	$e_{CT,Tissue}$	$P_{Pairwise}$	$P_{Independent}$
Averaging	64.2 ± 26.0	64.2 ± 26.0	1	1
DWT [6]	64.9 ± 26.1	63.9 ± 25.9	< 0.001	0.707
Contourlet [8]	73.4 ± 28.6	64.2 ± 24.9	< 0.001	0.083
Piella [19]	152.8 ± 52.6	175.9 ± 54.0	0.002	0.006
Graph Cuts	46.6 ± 12.3	81.7 ± 52.6	0.006	0.020
Method	$e_{CT,Bone}$	$e_{MR,Bone}$	$P_{Pairwise}$	$P_{Independent}$
Averaging	82.5 ± 19.8	82.5 ± 19.8	1	1
DWT [6]	81.9 ± 19.7	83.7 ± 19.8	< 0.001	0.583
Contourlet [8]	82.6 ± 19.7	89.0 ± 18.6	< 0.001	0.121
Piella [19]	84.1 ± 40.6	188.7 ± 48.0	< 0.001	< 0.001
Graph Cuts	57.0 ± 11.9	108.0 ± 36.2	< 0.001	< 0.001

Table 2: MEAN SENSITIVITY FOR TISSUE AND BONE DETAILS ALONG WITH MEAN SSIM INDEX MEASURES FOR ALL FIVE METHODS.

Method	Sensitivity Tissue	Sensitivity Bone	SSIM Tissue	SSIM Bone
Averaging	0 ± 0	0 ± 0	0.59 ± 0.32	0.08 ± 0.04
DWT [6]	0.51 ± 0.01	0.76 ± 0.17	0.54 ± 0.32	0.11 ± 0.06
Contourlet [8]	0.50 ± 0.01	0.75 ± 0.17	0.22 ± 0.30	0.12 ± 0.08
Piella [19]	0.86 ± 0.11	0.87 ± 0.08	0.32 ± 0.31	0.15 ± 0.11
Graph Cuts	0.63 ± 0.12	0.84 ± 0.09	0.52 ± 0.33	0.21 ± 0.12

9. CONCLUSION

They are many ways of fusing images. We have compared the regular image fusion techniques with the weighting graph cuts(WGC) Algorithm based techniques. It can be seen from the above table and the image results that the WGC based techniques are having much better results when compared with the conventional techniques.The WGC based image fusion algorithms are introduced and their objective and subjective comparison with other classical techniques is carried out. It is concluded from experimental results that WGC based image fusion schemes perform better than existing schemes.

10. REFERENCES

[1]Y. Hu, S. K. Mirzac, J. G. Jarvikb, P. J. Heagerty, and D. R. Haynor, "MR and CT image fusion of the cervical spine: A noninvasive alternative to CT-Myelography," in *Proc. SPIE,* 2005, vol. 5744.

[2]Y. Boykov, O. Veksler, and R. Zabih, "Fast approximate energy mini-mization via graph cuts," *IEEE Trans. Pattern Anal. Mach. Intell.*, vol. 23, no. 11, pp. 1222–1239, Nov. 2001

[3] M. B. Salah, A. Mitiche, and I. B. Ayed, "Multiregion image segmentation by parametric kernel graph cuts," *IEEE Trans. Image Process.*, vol. 20, no. 2, pp. 545–557, Feb. 2011.
[4] P. Hill, N. Canagarajah, and D. R. Bull, "Image fusion using complex wavelets," in *Proc. Brit. Mach. Vis. Conf.*, 2002.